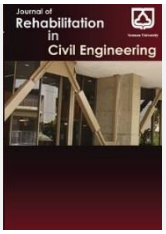

Journal of Rehabilitation in Civil Engineering

Journal homepage: https://civiljournal.semnan.ac.ir/

Design Optimization of Strongback Braced Steel Frames Incorporating a Novel Drift Uniformity Constraint

Ehsan Jahankhani [1]; Omid Rezaifar [2,*]; Majid Gholhaki [3] ; Peyman Homami [4]

1. Ph.D. Candidate, Department of Civil Engineering, Semnan University, Semnan, Iran
2. Professor, Faculty of Civil Engineering, Semnan University, Semnan, Iran
3. Professor, Faculty of Civil Engineering, Semnan University, Semnan, Iran
4. Associate Professor, Faculty of Civil Engineering, kharazmi University, Tehran, Iran

* Corresponding author: *orezayfar@semnan.ac.ir*

ARTICLE INFO

Article history:
Received: 04 November 2025
Revised: 03 December 2025
Accepted: 23 December 2025

Keywords:
Optimization;
Strong back;
Steel structure;
GA (Genetic Algorithm).

ABSTRACT

This study investigates the optimal seismic design of a six-story steel frame equipped with three Strongback bracing configurations, characterized by brace-to-beam intersection ratios of $\frac{1}{4}$, $\frac{1}{3}$, and $\frac{5}{12}$ of the span. A Genetic Algorithm (GA) developed in MATLAB was integrated with OpenSees to perform linear static analyses while enforcing a set of design constraints, one of which is a newly introduced drift-uniformity constraint aimed at regulating the distribution of inter-story drifts. A comparative assessment of the three configurations reveals distinct behavioral trends. In the unconstrained optimization, the differences in total structural weight among the configurations remain moderate 0.61% between $\frac{1}{3}$ and $\frac{1}{4}$ span, 12.27% between $\frac{1}{3}$ and $\frac{5}{12}$, and 11.73% between $\frac{1}{4}$ and $\frac{5}{12}$. When the drift-uniformity constraint is included, these differences increase to 4.17%, 25.56%, and 28.55%, respectively, highlighting the pronounced sensitivity of Strongback systems to geometric configuration and showing that brace-to-beam intersection location plays a decisive role in their stiffness-redistribution behavior. The effect of the drift-uniformity constraint varies across the three configurations: it leads to weight reductions of 2.47% and 6.95% in the $\frac{1}{4}$- and $\frac{1}{3}$-span arrangements, respectively, while producing a moderate increase of 14.96% for the $\frac{5}{12}$ span case. Despite this variation, all three systems exhibit improved drift profiles when the constraint is applied. Overall, the findings demonstrate that geometric configuration strongly influences the efficiency of Strongback action, and the proposed drift-uniformity constraint serves as an effective and novel design feature capable of refining drift distribution while maintaining competitive structural weight.

E-ISSN: 2345-4423

How to cite this article:
Jahankhani, E., Rezaifar, O., Gholhaki, M. and Homami, P. (2026). Design Optimization of Strongback Braced Steel Frames Incorporating a Novel Drift Uniformity Constraint. Journal of Rehabilitation in Civil Engineering, 14(3), 2515. http://doi.org/10.22075/jrce.2025.2515

1. Introduction

Improving the seismic performance of lateral load resisting systems has become a critical focus in modern structural engineering, particularly in the rehabilitation of vulnerable structures [1,2]. Among the various systems developed to enhance seismic resilience, the Strongback system has attracted increasing interest due to its capability to redistribute story drifts more uniformly and prevent soft story mechanisms during seismic events [3,4].

The Strongback system introduces a vertical spine or stiffening element into the structural frame, allowing for better control of deformation patterns and enhancing energy dissipation [5,6]. While several studies have investigated the general behavior of Strongback equipped frames, research specifically focused on the optimization of these systems remains relatively limited. In particular, few studies have explored optimization frameworks that incorporate practical design constraints such as drift uniformity, which plays a vital role in minimizing localized damage during seismic events [4].

To address this gap, the present study introduces a novel constraint into the optimization process: the uniformity of inter story drift distribution. This constraint aims to minimize the concentration of deformation in specific stories, thereby improving the overall seismic performance and post earthquake reparability of the structure.

To achieve optimal design configurations, a genetic algorithm was employed within a MATLAB environment, integrated with OpenSees for structural analysis. Linear static analysis was used to evaluate the lateral performance of the structural models, and the optimization objective focused on minimizing peak inter story drift while satisfying the drift uniformity constraint.

This study proposes a constraint driven optimization framework that not only improves seismic response but also addresses a research gap in the existing literature. The findings are expected to provide new insights into the application of Strongback systems in seismic rehabilitation and inform future design strategies for resilient building structures.

in recent decades, structural optimization has emerged as a pivotal area in earthquake resistant design, with particular emphasis on performance based engineering and cost efficiency. Among the various metaheuristic methods, the GA has proven to be an effective and flexible tool in solving complex optimization problems involving discrete variables and nonlinear constraints. GA has been widely applied to the optimal design of trusses [7], steel frames [8], reinforced concrete structures [9], and bracing systems [10–12], aiming to minimize structural weight while satisfying design constraints such as strength, buckling, and serviceability.

Several studies have also explored the use of GA in the seismic design of structures [13–15], particularly for optimizing lateral force resisting systems under static or dynamic loading. These applications typically focus on satisfying traditional constraints like strength and drift limits, yet they often overlook modern performance based criteria such as inter story drift uniformity, which is crucial in preventing soft story mechanisms and local failures [16–18] consequently, there is a growing interest in integrating intelligent optimization with innovative structural systems to better control lateral deformations in seismic design.

One of the most promising developments in [16] this regard is the Strongback bracing system, first introduced by Lai and Mahin [5]. The system was designed to reduce concentration of inelastic deformations in steel braced frames by incorporating a vertical elastic spine that remains elastic during seismic events. The spine, composed of vertical truss or beam elements, distributes lateral displacements uniformly along the building height and reduces soft story formation. Lai and Mahin recommended limiting the stress ratio in spine members to 0.5 to ensure elastic behavior and improve drift uniformity.

Following this concept, several researchers proposed modifications to the Strongback system. Panian et al. [19] introduced a new configuration using buckling restrained braces (BRBs) as inelastic members. Their study on a four story model demonstrated that the spine system could enhance redundancy and eliminate structural indeterminacy. Laqi et al. [20,21]investigated the effect of connection types by comparing spine systems with rigid and pinned joints, finding that moment resisting frames experienced lower base level stresses than pinned ones.

Liu [22] developed a rotational Strongback system using self centering dampers and fuse links, providing around 20% of the lateral strength through the spine, while the remaining portion was supported by BRBs. Palermo et al. [23] emphasized the role of beam to column stiffness ratio in stress distribution, where stiffer beams reduced lower story demands and softer beams transferred forces upwards.

Experimental and numerical investigations confirmed the improved seismic performance of Strongback systems. Simpson and Mahin [6] conducted FEMA P695 based studies on a four story Strongback frame, revealing better drift distribution and reduced collapse probability compared to BRB only frames. In another study [3], they showed that even after BRB core rupture, the elastic spine maintained lateral control through force redistribution.

Tully [24] promoted capacity based modal design for Strongbacks, leading to improved force distribution. Lin et al [25] evaluated the effect of spine stiffness in reducing inter story drift in RC buildings. Salek Faramarzi et al, [26] proposed a direct Performance based design using yield frequency spectrum, achieving 98% convergence in OpenSees and a 20% higher median collapse capacity than code based design.

Higher mode effects in tall buildings were addressed by Simpson [27], who found that elastic spines effectively distributed modal forces and reduced soft story formation. Toorani et al. [4] analyzed Strongback systems under sequential near and far fault ground motions, identifying that optimal stiffness ratio between elastic and inelastic braces improved drift uniformity across various building heights. Toorani et al. were the first to introduce the drift uniformity index. However, they did not pursue optimization in their work and, consequently, did not define a Drift Uniformity Factor (DUF) constraint to explore its impact on structural optimization, weight reduction, and the redistribution of forces and stiffness. Therefore, the present paper investigates a constraint inspired by the drift uniformity index from Toorani et al. work. The DUF concept is also derived from this same index. The drift-uniformity constraint introduced in this study is formulated to regulate inter-story drift distribution by limiting excessive concentration in any single story. This constraint directly targets soft-story formation and enhances the seismic performance of the system. A brief numerical illustration is later provided to clarify its practical impact.

Smart materials such as SMAs have also been shown to reduce residual drift and promote more uniform interstory deformation patterns, further emphasizing the importance of drift-management strategies such as those examined here [28].

In addition to structural systems, supplemental damping technologies have also advanced significantly. Recent studies on steel bar hysteretic dampers (SBHDs) have shown that properly calibrated hysteretic devices can greatly enhance the energy-dissipation capacity of isolated systems, with reliable predictive models developed using nonlinear regression. These findings further emphasize the importance of regulating drift and deformation demands an emphasis consistent with the present study [29].

Faramarzi and Touraj [30] emphasized the influence of brace to beam intersection location, showing that placing it at two thirds of the beam length improved ductility and reduced drift by 30%. Astudillo et al. [31] compared Strongback to conventional BRB Chevron systems, reporting better drift control and energy dissipation in the Strongback frames.

Abolghasemi et al. [32] demonstrated that in damped buildings, Strongback reduced drift sensitivity to damper configuration. Recent advances have also explored hybrid strong-back configurations that combine vertical strong-back trusses with shear-link fuses to eliminate soft-story formation and enhance global energy dissipation. Nonlinear cyclic and time-history analyses have demonstrated that such hybrid systems can successfully delay drift concentration and fully engage shear links along the building height, offering further evidence of the effectiveness of drift-management strategies relevant to the present study [33]. Gholhaki et al. [34] retrofitted 5, 10, and 15 story RC frames using Strongback and reported 33%–44% reduction in inter story drift.

Recent studies have increasingly focused on developing innovative bracing and energy-dissipation mechanisms to improve seismic resilience and mitigate excessive drift concentration in steel frames. Among these advances, elliptic-braced moment-resisting frames equipped with rotational friction dampers (ELBRF-RFD) have been proposed as an effective displacement-restraint system capable of enhancing structural ductility and collapse resistance. Through nonlinear static and incremental dynamic analyses, this system has demonstrated significant improvements in seismic performance factors and reduced collapse probability compared to conventional braced frames. Such research highlights the growing interest in bracing configurations that improve drift distribution and promote more uniform structural response an objective aligned with the motivation of the present study, which investigates drift-regularizing mechanisms within Strongback braced frames [35].

Recent advances in innovative bracing systems, including multi-story Elliptic-Braced Resisting Frames (ELBRF) and their enhanced Mega-ELBRF counterparts, have shown improved ductility, stable hysteresis, and reduced collapse probability through laboratory and numerical investigations. These systems emphasize the importance of deformation-uniformity and drift mitigation in seismic design. Such trends further motivate the present work, which aims to enhance drift distribution in Strongback braced frames [36].

Recent advances have also emphasized the importance of system-specific loading protocols for accurately characterizing seismic deformation demands. Studies developing tailored protocols for different structural systems have shown that generalized loading histories may misrepresent drift patterns and cumulative damage, highlighting the necessity of precise deformation modeling an aspect that closely aligns with the drift-focused objectives of the present work [37].

Complementing earlier experimental studies on ELBRF/MELBRF systems, recent work on multi-story Elliptic and Quasi-X Braced Resisting Frames has further shown that advanced brace geometries can substantially enhance stiffness, ductility, and energy dissipation, while delaying failure progression. These results reinforce the relevance of deformation-modifying bracing strategies and provide additional motivation for the drift-uniformity-oriented Strongback framework developed in this study [38].

Recent studies have also demonstrated the effectiveness of supplemental energy-dissipation systems in controlling seismic demands. For example, the use of innovative Arc and Ring Dampers (ARDs) has been shown to significantly enhance drift performance, reduce residual deformations, and lower expected losses in deficient steel moment frames under the FEMA P-58 methodology [2]. These results further emphasize the growing focus on drift management and performance-based control strategies, aligning with the motivation of the present work [39].

Complementing these recent advances, mega elliptic-braced moment-resisting frames (MELBRFs) have also been investigated through rigorous FEMA P695 seismic performance factor evaluations [40]. MELBRFs combine special moment frames with mega-scale elliptic braces to improve ductility, overstrength, and collapse safety while reducing structural weight and preserving architectural openness. Nonlinear analyses across multiple archetype heights have confirmed acceptable collapse margin ratios and a response modification factor of 6.5, demonstrating the efficiency of this emerging dual lateral

system. These developments collectively highlight the increasing emphasis on systems capable of regulating drift patterns and improving story-wise deformation performance an emphasis that aligns directly with the objectives of the drift-uniformity optimization strategy proposed in this study [41].

Parallel to structural innovations, optimization-based approaches have gained increasing attention in seismic engineering. Notably, recent studies employing the improved Prairie Dog Optimization (I-PDO) algorithm have demonstrated its effectiveness in both topology and size optimization of steel mega-braced frames, achieving enhanced stiffness, stability, and lateral load distribution. These efforts underscore the importance of metaheuristic optimization in refining seismic performance, providing further context for the optimization-driven methodology adopted in the present research [42].

The proposed drift-uniformity constraint differentiates this study from earlier optimization research, which rarely incorporated explicit drift-distribution control.

Despite these advancements in the structural behavior and design of Strongback systems, limited studies have incorporated them within optimization frameworks, particularly using Genetic Algorithms. Most previous research evaluated the performance of Strongback configurations post design rather than including them as decision variables during optimization. To date, no study has simultaneously addressed seismic performance, weight minimization, and inter story drift uniformity as explicit constraints in optimizing Strongback equipped frames. This study aims to fill that gap by employing a Genetic Algorithm to optimize steel frames with Strongback bracing systems, subject to constraints on strength, buckling, deformation, and drift uniformity.

1.1. Significance and Research Scope

This study pursues a focused, comparative aim: to quantify how inter story drift uniformity influences optimal section selection and total cost in steel frames retrofitted with Strongback bracing. Rather than a routine weight minimization exercise, the work targets a higher level question why and where enforcing drift uniformity changes design decisions and economic outcomes and provides a metric and framework to answer it. The analyses are carried out under an equivalent linear assumption because Strongback systems are intended to preserve near linear response up to performance limits; consequently, the linear results are directly useful for preliminary engineering design and economic assessment. Finally, the proposed index and optimization framework establish a transferable basis for future, more comprehensive studies (e.g., nonlinear static and time history analyses) that will validate and extend the findings into fully nonlinear performance regimes.

1.2. Research Gap and Motivation

Although Strongback systems have been shown to improve drift distribution and delay soft-story formation, existing studies have rarely examined how design optimization might enhance their performance. Prior research has primarily focused on predefined configurations, leaving the influence of geometric parameters, such as the brace-to-beam intersection location, insufficiently quantified. More importantly, no optimization-based study has incorporated a drift uniformity oriented design constraint, even though the Drift Uniformity Index originally introduced by Toorani et al. [4] demonstrated the importance of controlling drift concentration in frame structures.

Another gap in the literature is the absence of a systematic, algorithm-driven framework capable of evaluating different Strongback geometries under practical design constraints. The combined effect of frame configuration and drift-uniformity requirements remains unexplored, and there is limited evidence on how these factors interact to influence structural weight, efficiency, and seismic deformation patterns.

Motivated by these gaps, the present study develops an integrated GA–OpenSees optimization platform and investigates how incorporating a DUF based constraint affects the optimal behavior of Strongback frames with different brace-to-beam intersection ratios. This provides the first quantitative evaluation of

how drift-uniformity-driven optimization interacts with Strongback geometry, addressing a clear gap in prior research.

2. Materials and Methods

To investigate the seismic performance and optimize the design of steel frames equipped with Strongback bracing systems, a comprehensive computational framework was developed. The study focused on a six story steel braced frame subjected to three different Strongback configurations, distinguished by the location of the brace to beam intersection (at $\frac{1}{4}$, $\frac{1}{3}$, and $\frac{5}{12}$ of the span length) [4]. Structural analysis was carried out using linear static procedures in OpenSees, while optimization was performed in MATLAB using a Genetic Algorithm. The objective was to minimize structural weight while satisfying constraints related to strength, buckling, lateral deformation, and a newly introduced constraint on inter story drift uniformity. Full integration between analysis and optimization modules enabled automated and efficient evaluation of candidate solutions throughout the process.

The structural model investigated in this study is a two dimensional, six story, three bay steel frame equipped with Strongback bracing systems. Each bay has a clear span length of 9.14 m. The first story height is 5.49 m, while each of the remaining five stories has a uniform height of 3.96 m. Three distinct Strongback configurations were examined, differentiated by the brace to beam intersection location: at one quarter ($\frac{1}{4}$), one third ($\frac{1}{3}$), and five twelfths ($\frac{5}{12}$) of the beam span. These configurations are illustrated in Figure 1, which presents the elevation views of the six story frame for the three investigated layouts. The structural model of the six story frame and the member grouping scheme used for defining the 19 design variables are illustrated in Figure 1. The three Strongback configurations investigated in this study are shown in Figure 1(a–c).

he selected ratios ($\frac{1}{4}$, $\frac{1}{3}$, and $\frac{5}{12}$) reflect meaningful variations in the brace force path and beam shear–moment interaction. The $\frac{1}{4}$ ratio engages higher shear transfer, the $\frac{1}{3}$ ratio offers balanced stiffness segmentation, and the $\frac{5}{12}$ ratio increases the bending-dominated response. These choices are also consistent with prior studies [13,24].

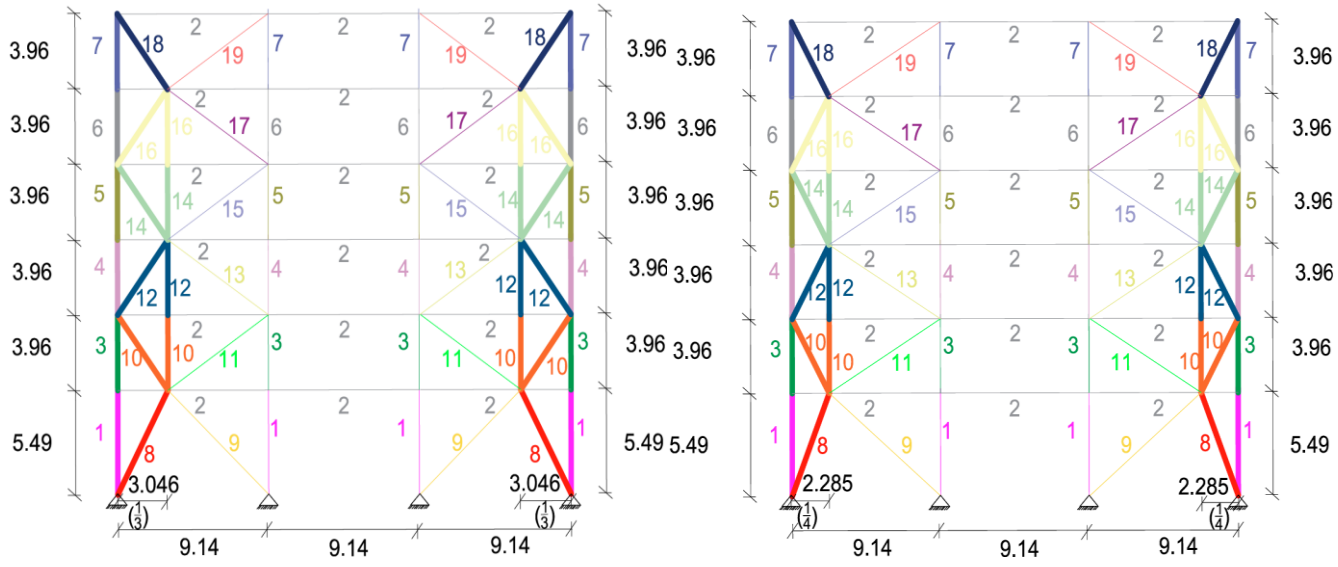

(a) (b)

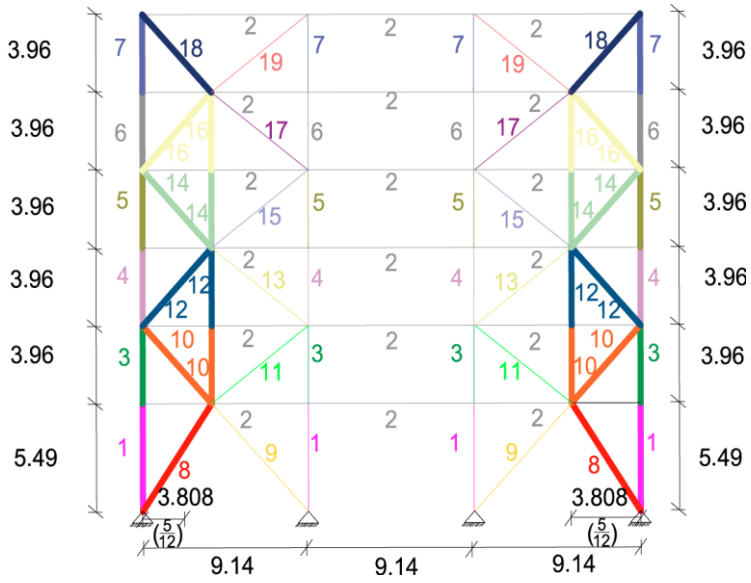

(c)

Fig. 1. Structural configuration of the six-story Strongback braced frame for the three brace-to-beam intersection ratios ($\frac{1}{4}$, $\frac{1}{3}$, and $\frac{5}{12}$ of the span).

Figure 1 illustrates the three Strongback configurations analyzed in this study. These configurations were selected to represent distinct stiffness interaction mechanisms between the braced and unbraced portions of the frame. The one third span layout provides a balanced stiffness transfer along the height All units in Figure 1 are expressed in meters (m) for dimentions.

All beam to column and brace to beam connections were modeled as pinned joints and column bases were assumed to be pined. Structural members were selected from standard W and HSS steel sections. Strongback elements were modeled as purely elastic members to maintain stiffness and facilitate uniform drift distribution during seismic events. Table 1 presents the mechanical properties assigned to the steel sections used in all numerical analyses.

Table 1. Mechanical properties assigned to the steel members in the analytical models**.**

Name of peroperty	symbol	Parameter value
density	ρ (kg/m^3)	7850
Elastic modulus	E (MPa)	200000
Yield strength	f_y (MPa)	317

As indicated in Table 1, the selected mechanical properties are representative of conventional structural steel used in seismic design, thereby providing appropriate stiffness, yield behavior, and mass characteristics for the modeled Strongback systems.Gravity loads were applied as follows: floor dead load of 5500 N/m², floor live load of 2000 N/m², roof dead load of 6100 N/m², and roof live load of 1500 N/m². Seismic loading was determined in accordance with the design spectrum parameters for site classes Type II and Type III soils, with Ru(Response Modification factor (behavior factor)) = 6, I (Importance factor)= 1, A (Design Base Acceleration coefficient (Spectral acceleration at short period))= 0.35, and cd (Displacement Amplification factor) = 5.2. [13,25] The maximum allowable lateral displacement at each joint was limited to 0.02 m. Additional design constraints included axial and flexural strength limits for columns, combined axial and bending checks for beams, compression and buckling checks for braces, and the drift uniformity constraint for the optimization cases.

To clearly illustrate the Strongback configuration and the location of brace-to-beam intersections adopted in this study, the overall structural layout is shown in Figure 2.

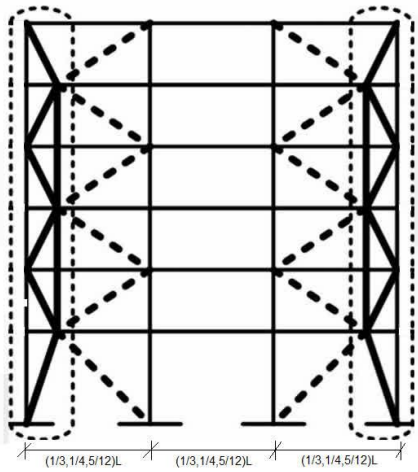

Fig. 2. Structural configuration of the Strongback braced frame with brace-to-beam intersection ratios of $\frac{1}{4}$, $\frac{1}{3}$, and $\frac{5}{12}$ of the span.

As shown in Figure 2, the Strongback elements are placed along the two exterior bays, forming a continuous vertical spine that constrains the deformation profile. The three investigated brace-to-beam intersection ratios $\frac{1}{4}$, $\frac{1}{3}$, and $\frac{5}{12}$ of the beam span are indicated along the base of each bay. These geometric variations define the effective brace angle and influence the global drift distribution, which are later evaluated through the optimization framework. The regions enclosed by the dotted outlines represent the Strongback elements of the system, while the members shown with dashed lines correspond to the energy dissipating braces that yield and form part of the intended structural mechanism. in Figure 2, L is length of span.

The selected brace-to-beam intersection ratios ($\frac{1}{4}$, $\frac{1}{3}$ and $\frac{5}{12}$ span) follow the configurations adopted by Toorani et all. [4], who applied the same proportions in their numerical Strongback frame study. Similar geometric ratios ($\frac{1}{2}$ and $\frac{1}{3}$) were also investigated by Lai and Mahin [5]. The present study therefore adopts these ratios to maintain consistency with previous research and to capture a representative spectrum of brace geometries for comparative evaluation.

The numerical analysis of the proposed frames was carried out using the OpenSees platform. A two dimensional linear static analysis was adopted to evaluate the structural performance under seismic and gravity loading conditions. No dynamic analyses, such as response spectrum or time history procedures, were performed in this study. All structural members were modeled with linear (two linear) elastic material behavior to be consistent with the adopted analysis method.

Beam, column, and Strongback elements were represented using elastic beam–column elements with the specified cross sectional and material properties described in Section 2.1. All beam to column and brace to beam connections were modeled as idealized pinned joints and column bases were assumed to be hinged. The Strongback members were modeled as purely elastic components, ensuring that they remained undeformed beyond the elastic range and acted as stiff vertical spines to control inter story drift distribution.

Second order effects (P–Δ) were neglected in the analysis, given the linear static approach and the service level load conditions considered. The gravity loads were applied as uniformly distributed loads on beams, while seismic lateral forces were calculated using equivalent static load procedures in accordance with the relevant design code parameters. The load combination adopted for the analysis incorporated dead load, live load, and seismic effects.

This modeling approach allowed for efficient integration with the optimization algorithm implemented in MATLAB, facilitating rapid evaluation of numerous design candidates while ensuring compliance with the defined strength, buckling, deformation, and drift uniformity constraints.

The optimization and structural evaluations presented herein employ linear static analysis (equivalent static seismic loading) as an efficient and robust tool for comparative exploration of discrete section choices and brace geometries across a large design space. It should be noted that this elastic approach is most appropriate for preliminary design and screening, particularly in cases where the Strongback spine is intentionally proportioned to remain elastic up to the targeted performance level, as recommended in prior studies [4].

However, linear analysis cannot capture post-yield phenomena such as strength degradation, redistribution of internal forces due to plastic hinging, residual drifts, or cyclic energy dissipation. Consequently, the quantitative effectiveness of the DUF under severe inelastic demand cannot be fully validated within the present elastic framework. In view of this limitation, the DUF is here interpreted as an elastic stage regularizer that promotes balanced stiffness allocation and delays the onset of localized plastic demands. A systematic nonlinear validation (nonlinear static pushover and selected nonlinear time-history analyses) is necessary to assess the DUF's performance in the post-yield regime; a program to perform these analyses for representative optimized designs is planned as part of future researching work.

To effectively integrate the structural analysis and optimization stages, a computational framework was developed to enable automated evaluation of candidate designs. The process begins with defining the structural geometry, material properties, and member cross sections. Gravity and equivalent static seismic loads are then applied according to the design code provisions. The structural performance is evaluated through linear static analysis in OpenSees, and the results are checked against multiple design constraints, including strength, buckling, lateral deformation, and inter story drift uniformity. The optimization process, implemented in MATLAB using a Genetic Algorithm, iteratively updates the design variables until convergence to the optimal solution is achieved. The overall workflow of the proposed methodology is illustrated in Figure 3.

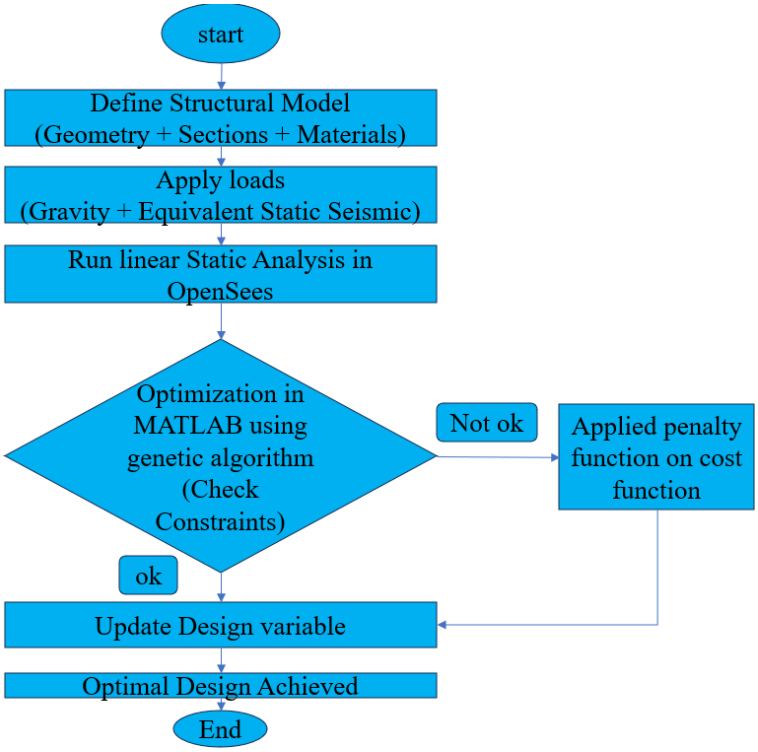

Fig. 3. Flowchart of the proposed MATLAB–OpenSees optimization framework using a Genetic Algorithm for Strongback system design.

Figure 3 clearly illustrates the geometric configuration and the member grouping scheme adopted for the optimization. This systematic grouping not only reduces the dimensionality of the design space but also ensures that members with similar load and deformation characteristics share consistent section properties, improving both computational efficiency and structural regularity.

2.1. Optimization Framework

The optimization problem in this study is formulated as a discrete size optimization, where each design variable corresponds to the cross sectional size of a specific member group in the structural model. A total of 19 design variables were considered, representing the 19 member groups in the frame. The section sizes were selected from a predefined database of 263 standard W and HSS steel profiles. The optimization problem is formulated as a discrete size optimization aiming to minimize the total structural weight, as expressed in Equation (1) [8].

Minimize: $= w_{total} = \sum_{j=1}^{19} n_j L_j A_j \rho_j$ (1)

where ρ_j is the steel density, A_j is the cross sectional area of the jth section type, L_j is the mem ber length, and n_j is the number of members using that section type.

The following constraints are imposed during the optimization process:

- Strength constraints — axial, flexural, and combined axial–flexural strength checks according to the relevant steel design code.

- Buckling constraints — elastic and inelastic buckling limits for compression members.

- Maximum inter story drift constraint — to limit lateral deformations and ensure serviceability.

- Drift uniformity constraint — a novel performance criterion introduced in this study to control the distribution of inter story drift along the height, improving seismic performance.

$$\begin{cases} 1.\,Strength\ constraints \begin{cases} 1.\,axial \text{ strength} \\ 2.\,flexural \text{ strength} \\ 3.\,combined\ axial-flexural\ strength \end{cases} \\ 2.\,overall\ buckling\ of\ the\ element\ \ constraints \\ 3.\,Local\ buckling\ of\ the\ element\ \ constraints \\ 4.\,Maximum\ inter-story\ drift\ constraint \\ 5.\,Drift\ uniformity\ constraint \end{cases}$$

The seismic design constraints, including the maximum inter-story drift and story displacement limits, were defined according to the provisions of the Iranian Seismic Code (Standard No. 2800, 4th Edition, 2015) [43]. This code specifies that the amplified story drift, obtained by multiplying the computed elastic drift by the displacement amplification factor, should not exceed 0.02 of the story height.

The optimization was performed using a GA implemented in MATLAB, fully integrated with OpenSees for structural analysis. Candidate solutions were evaluated using linear static analysis, with automated data transfer between the analysis and optimization modules. The GA implementation details are as follows:

- Number of design variables: 19

- Initial population size (Np): 280 individuals, randomly generated from the discrete section database

- Selection operator: Roulette Wheel selection

- Crossover operators: Single point and double point crossover, chosen randomly

- Mutation rate: 0.2, applied to randomly selected genes to maintain diversity

- Termination criterion: 100 generations

Optimization Procedure:

The process begins with the generation of an initial random population of Np = 280 chromosomes. Each chromosome consists of 19 genes, corresponding to the discrete design variables representing the section sizes of the member groups. Gene values are selected from the 263 section database using randomly generated integer masks with bounds between 1 and 263, determining the position of each gene in the design space. The optimization process was conducted using a discrete pool of 263 W and HSS sections, whose statistical characteristics are summarized in Table 2.

Once the chromosomes are generated, each is mapped to a structural model in which member section sizes are assigned according to the chromosome's genes. The structural geometry is created in MATLAB and exported to an OpenSees input script, where a linear static analysis is conducted. The resulting nodal displacements and member stresses are returned to MATLAB for constraint verification and objective function evaluation.

The cost function is defined as the total structural weight, with penalty terms added when any constraint is violated. These penalties increase the cost value, lowering the probability of selecting infeasible solutions.

Table 2. Statistical characteristics of the steel section pool considered for the optimization process.

	Area	I
Minimum	(HSS2X2X1/8) 0.0005	(HSS2X2X1/8) 0.0000002
Maximum	(W36X652) 0.1242	(W36X652) 0.0211
Mean(average)	0.0241	0.0019
median	0.016	0.0004
variation	0.0005	0.000009
Standard deviation	0.0234	0.0031
Number of sections	263	

Table 2 summarizes the statistical characteristics of the steel section pool used in the optimization process. The database consists of 263 W and HSS sections covering a broad range of cross sectional areas and moments of inertia. The minimum and maximum values of the section area indicate the wide variability in available profiles, allowing the optimization algorithm to explore both lightweight and high capacity design options. Similarly, the large range in the moment of inertia values ensures sufficient flexibility in stiffness distribution during the optimization search.

The mean and median values demonstrate that the section pool is moderately skewed toward medium sized members, which provides a balanced foundation for both economical and structurally efficient solutions. The calculated standard deviations and variances further confirm a significant diversity among available profiles, preventing premature convergence of the Genetic Algorithm and enhancing the robustness of the search process.

Overall, the statistical characteristics presented in Table 2 reflect a well defined and diverse section pool that enables the proposed optimization framework to effectively balance weight minimization with structural performance requirements.

After evaluation, chromosomes are ranked by their cost values (lower is better). Parent chromosomes are selected using the Roulette Wheel operator based on their relative fitness. Crossover is performed using either single point or double point methods (chosen randomly) to generate offspring. A two parent, two offspring strategy is adopted, and this process continues until the offspring population reaches size Np.

Mutation is then applied to individuals selected via Roulette Wheel, with a mutation rate of 0.2, where one or more genes are randomly altered. This produces an additional population of size Np. The original population, crossover offspring, and mutation offspring are combined into a pool of 3Np individuals. This combined population is sorted by cost function value, and the top Np individuals are retained as the next generation.

The best solution from each generation is recorded for performance monitoring. This iterative process continues until the stopping criterion reaching 100 generations is satisfied.

A maximum of 100 generations was adopted as a conservative termination limit to ensure stable convergence in all cases. Several trial runs with different random initial populations showed highly similar final fitness values, indicating that the optimization results are reproducible and insensitive to initial randomization.

Figure 4 illustrates the flow of the GA applied in this study. The process starts with the random generation of an initial population of discrete design solutions. Each individual is evaluated via structural analysis, and penalties are applied for constraint violations. Selection is performed using the Roulette Wheel method, followed by crossover (single or double point) and mutation operations to generate new designs. The best solutions are carried forward to the next generation. The process repeats until the stopping criterion of 100 generations is met.

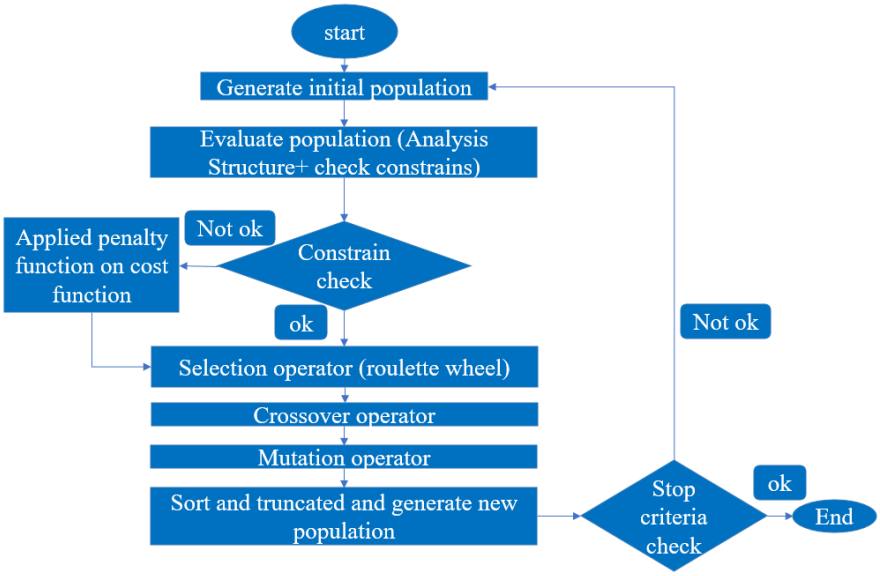

Fig. 4. Flowchart of the GA optimization procedure used in this study.

2.2. Definition of Novel Drift Uniformity Constraint

In seismic design, inter story drift is a critical parameter that governs the deformation capacity and overall performance of structures under lateral loading. Current design codes and guidelines, such as AISC 341 [1] and FEMA 356 [44], primarily impose limitations on the maximum allowable drift to prevent excessive lateral displacements and to ensure serviceability. However, these provisions do not explicitly address the distribution of drift along the height of the structure. In many cases, non uniform drift patterns may occur, leading to undesirable effects such as soft story mechanisms or concentration of deformations

in specific stories. These irregularities can significantly compromise seismic performance and increase the likelihood of structural damage or collapse.

Despite the importance of controlling maximum inter story drift, conventional design approaches often overlook the uniformity of drift distribution. As a result, buildings may satisfy the code based drift limits while still experiencing highly irregular drift profiles, where one or more stories undergo significantly larger deformations compared to adjacent stories. This phenomenon, commonly referred to as the "soft story" effect, can lead to severe structural and non structural damage, concentration of inelastic demands, and in extreme cases, partial or total collapse. Therefore, ensuring a more uniform distribution of inter story drift is essential to enhance structural resilience and improve seismic performance.

To address the limitations of conventional drift based design, this study introduces a novel *Drift* Uniformity Constraint. Rather than restricting only the maximum inter story drift, the proposed criterion explicitly governs the regularity of the drift profile along the building height. The degree of uniformity is quantified through a dedicated (DUF), defined as the ratio of local story drift to the global average drift demand (see Equation 3). Maintaining this factor within a narrow permissible range (e.g., $0.9 \leq$ DUF $\leq$ 1.1) ensures a highly uniform deformation pattern, whereas deviations beyond this interval indicate irregular drift concentrations or potential soft story behavior. The optimization algorithm enforces this constraint by penalizing candidate solutions exhibiting excessive drift non uniformity, thereby steering the search toward configurations that achieve both global stability and improved seismic performance.

Each chromosome consists of 19 genes, corresponding to the discrete design variables representing the section sizes of member group.

discrete optimization vector, representing the sectional configuration of the 19 member groups, is defined in Equation (2) [8], where each variable $x_j$corresponds to a section type selected from the 263 available profiles in the database.

$$x = \{x_1, x_2, \ldots, x_{19}\}, x_j = \{1,2,\ldots,263\} \tag{2}$$

Each design variable xj represents the discrete index of a W or HSS section selected from the section database. The DUF is formulated as shown in Equation (3) [4] The proposed DUF is defined in Equation (3) as the normalized ratio between local and global drift demands.

Novel drift uniformity constraint (proposed):

$$0.9 \leq \left| \frac{(\frac{d2-d1}{hs})}{(\frac{dr}{H})} \right| \leq 1.1 \tag{3}$$

In equation (3), the parameters d2, d1, hs, dr, and H are the displacement of the upper floor, the displacement of the lower floor, the height difference between the upper and lower floors (floor height), the displacement of the roof, and the height of the entire structure, respectively. The parameters used in Eq. (3) are graphically illustrated in Figure 5 to clarify the geometric definition of the DUF. The geometric representation of these parameters is shown in Figure 5, where d_1, d_2, h_s, d_r, and H denote the story displacements, story height, roof displacement and total structure height, respectively. the threshold range (0.9–1.1) was adopted based on preliminary parametric calibration.The geometric parameters defining the DUF are schematically shown in Figure 5 to illustrate the physical meaning of Equation (3). The target range for the DUF was selected based on a set of preliminary parametric calibration studies aimed at balancing drift uniformity enhancement and structural efficiency. Several DUF bands namely 0.85–1.15, 0.90–1.10, and 0.95–1.05 were examined to assess the sensitivity of the optimization outcomes. The interval of 0.90–1.10 was found to provide the most effective compromise: it ensured that

the inter-story drift distribution remained nearly uniform (within ±10% variation) while maintaining a moderate increase in total structural weight. Tighter bounds such as 0.95–1.05 led to significantly higher weight penalties with limited uniformity improvement, whereas wider bounds such as 0.85–1.15 resulted in noticeable loss of drift control. Therefore, the DUF target range of 0.90–1.10 was adopted in this study as a practical and calibrated balance between seismic performance and structural economy.

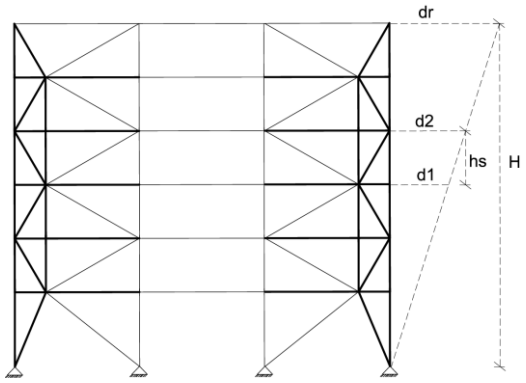

Fig. 5. Geometric definition of parameters used in the formulation of the proposed drift uniformity index.

The proposed drift uniformity constraint was incorporated into the optimization framework by extending the objective function with a penalty term associated with the *DUF*. In each iteration, after the structural analysis was completed in OpenSees, the inter story drift ratio for every story was calculated and compared with the overall roof drift ratio normalized by the total building height. For each story, the DUF was determined as the ratio of local to global drift demand, as defined in Equation (3). The deviation of each DUF from the target range ($0.9 \leq \text{DUF} \leq 1.1$) was then quantified, and a penalty proportional to the magnitude of this deviation was incorporated into the objective function.

This procedure ensured that candidate solutions exhibiting significant drift irregularities where one or more stories deviated beyond the acceptable DUF bounds received higher penalty values, reducing their likelihood of survival in subsequent generations. Conversely, designs maintaining nearly uniform drift patterns along the building height were assigned minimal penalties and thus retained a higher probability of reproduction and propagation through the evolutionary process. Through this mechanism, the Genetic Algorithm was efficiently guided not only to minimize the total structural weight but also to promote a balanced and stable lateral deformation profile, thereby enhancing the seismic reliability of the optimized Strongback braced frames.

To clearly illustrate the formulation of the proposed Drift Uniformity Index, the geometric definition of the parameters involved is presented in Figure 5. As shown, $d_1$and $d_2$represent the lateral displacements of the lower and upper story levels, respectively, while $h_s$denotes the story height. The global roof displacement and total building height are defined as $d_r$and H, respectively. The ratio $(d_2 - d_1)/h_s$represents the local inter story drift, and its normalization by the global drift ratio (d_r/H)forms the DUF used in Equation (3).

This schematic visualization facilitates understanding of how the DUF quantitatively captures the relative uniformity of story drifts along the building height and distinguishes between regular and concentrated deformation patterns.

It should be emphasized that although the DUF effectively regularizes elastic drift distributions, its direct extrapolation to inelastic behavior is not guaranteed. Inelastic mechanisms modify stiffness characteristics and modal participation, and therefore the DUF requires validation against nonlinear responses. For future verification, two complementary pathways can be adopted: (i) the DUF may be computed using target inelastic (yield-level) drifts obtained from pushover analyses or scaled inelastic demand spectra and subsequently incorporated into the optimization constraint; and (ii) incremental dynamic analyses (IDA)

may be performed on selected optimal designs to quantify performance metrics such as peak inelastic drift, residual drift, and collapse margin. Implementing these steps would enable a rigorous assessment of the DUF under severe seismic demands and facilitate potential recalibration of its threshold range for inelastic regimes.

2.3. Design Constraints and Mathematical Formulations

To provide a complete and transparent definition of the optimization problem, the mathematical formulations of all adopted design constraints are presented in this subsection. These constraints include strength limits, drift limits, slenderness requirements, member capacity checks, and DUF, which is introduced as an additional performance-oriented criterion. All constraint expressions follow relevant provisions of the AISC 341-16 [1] specification unless otherwise noted.

To prevent global instability in compression members and to ensure that all frame components satisfy the fundamental elastic stability requirements, an overall buckling constraint is imposed on each member. This constraint limits the slenderness ratio to acceptable bounds prescribed in steel design provisions, thereby avoiding premature global buckling under axial compression. The mathematical form of this stability requirement is expressed in Equation (4). to evaluate the global elastic stability of compression members and to establish a reference capacity against which axial demands can be compared, the classical Euler critical buckling load is computed. This load represents the theoretical maximum compressive force that an ideal prismatic member can sustain before experiencing elastic instability. The governing expression for the Euler buckling capacity is given in Equation (5). it is first constraint. In addition to the theoretical Euler load, the actual critical compressive strength of each member must account for effective length, boundary conditions, and geometric properties. Accordingly, a refined expression is employed to determine the practical critical axial capacity of the member under compression. This stability-based capacity, which governs the admissible axial demand-to-capacity ratio in the optimization process, is expressed in Equation (6).

$$g_1(x_i) = \max(\lambda_x, \lambda_y) - 200 < 0 \tag{4}$$

$$F_e = \frac{\pi^2 E}{\lambda^2} \tag{5}$$

$$\lambda > 4.71\sqrt{\frac{E}{f_y}} \rightarrow Fcr = 0.877F_e$$

$$\lambda < 4.71\sqrt{\frac{E}{f_y}} \rightarrow Fcr = f_y(0.658)^{(\frac{f_y}{Fe})}$$

$$Fcr = \min(f_y, Fcr) \tag{6}$$

In Equations (4-6), the parameters are defined as follows:

- λ_x and λ_y are the member slenderness ratios about the principal x- and y-axes, respectively.
- E denotes the modulus of elasticity of the steel.
- λ represents the governing member slenderness ratio.
- F_e is the Euler buckling stress.
- F_{cr} is the critical buckling stress.
- f_y is the steel yield stress.
- g signifies a constraint function within the optimization framework.
- x_i are the design variables for the optimization problem.

To establish the design compressive capacity of members subjected to axial compression, the nominal compressive strength is calculated based on the governing buckling limit state and material yielding. The corresponding expression is presented in Equation (7). The nominal tensile strength of tension-controlled members is evaluated by considering both yielding and potential rupture through the net cross-sectional area. The governing expression for the nominal axial tensile capacity is provided in Equation (8)

$$\mathrm{P_n} = \phi.\,\mathrm{Fcr}.\,\mathrm{A} \tag{7}$$

$$\mathrm{T_n} = \phi.\,\mathrm{f_y}.\,\mathrm{A} \tag{8}$$

In Equations (7) and (8), P_n and T_n denote the nominal axial compressive and tensile capacities, respectively, as defined by the governing steel design specification (AISC 3۴۱-16) [1]. A is area of section.

To ensure that all tension members remain within admissible axial limits, a tensile demand-to-capacity check is imposed. This constraint compares the factored axial tension force with the nominal tensile strength and prevents overstressing under design loads. The mathematical form of this constraint is given in Equation (9). For compression members, an additional constraint is introduced to ensure that the applied axial compressive force does not exceed the nominal compressive strength determined from buckling and yielding criteria. This compressive demand-capacity requirement is expressed in Equation (10).

$$g_2(x_i) = T_u - T_n < 0 \tag{9}$$

$$g_3(x_i) = P_u - P_n < 0 \tag{10}$$

The slenderness of the flange component is quantified to assess its susceptibility to local buckling under axial and flexural demands. The existing flange slenderness ratio is calculated according to Equation (11). Similarly, the slenderness of the web is evaluated to verify its stability against local buckling. The existing web slenderness ratio is determined using the expression in Equation (12). To classify the flange as compact, noncompact, or slender, the limiting slenderness threshold prescribed by design standards is applied. The limiting compactness criterion for the flange is given in Equation (13). A second limit associated with flange slenderness is considered to ensure elastic–plastic stability under combined axial and flexural actions. This slenderness requirement is defined in Equation (14). The limiting slenderness value for the web—used for stability classification and buckling checks is presented in Equation (15), in accordance with relevant design provisions. To enforce flange compactness within the optimization process, a constraint is imposed requiring the actual flange slenderness to remain below the prescribed limit. This requirement, representing the fourth design constraint, is formulated in Equation (16). Finally, to ensure adequate ductility and prevent premature local buckling, a compactness constraint is applied to the web. This condition requires the existing web slenderness to not exceed its allowable limit, as expressed in Equation (17).

$$\lambda_f = \frac{(b_f - t_w)}{\frac{t_f}{2}} \tag{11}$$

$$\lambda_w = \frac{d_c - 2t_f}{t_w} \tag{12}$$

$$\lambda_{Fp} = 0.38\sqrt{\frac{E}{f_y}} \tag{13}$$

$$\lambda_{Fr} = \sqrt{\frac{E}{Fy}} \tag{14}$$

$$\lambda_{wr} = 5.7\sqrt{\frac{E}{f_y}} \tag{15}$$

$$g_4(x_i) = \lambda_f - \lambda_{fp} < 0 \tag{16}$$

$$g_5(x_i) = \lambda_w - \lambda_{wp} < 0 \tag{17}$$

In Equations (11) to (17), the parameters are defined as follows:

- b_f: flange width
- t_f: flange thickness
- t_w: web thickness
- d_c: overall depth of the section
- λ_f: flange slenderness ratio
- λ_w: web slenderness ratio
- λ_{fp}: limiting slenderness for a compact flange
- λ_{fr}: limiting slenderness for a noncompact flange
- λ_{wr}: limiting slenderness for the web

To evaluate the global stability of compression members, the effective braced length must be quantified based on their bracing conditions and lateral support intervals. The expression used to determine the maximum effective braced length is provided in Equation (18). The stability of a compression member depends strongly on its radius of gyration, which governs its slenderness ratio and susceptibility to global buckling. The radius of gyration for the compression region of the cross-section is calculated using Equation (19). To facilitate stability and bending capacity calculations, the total depth of the structural section is defined. This geometric quantity, representing the full cross-sectional height, is expressed in Equation (20). The unbraced length of a member plays a critical role in determining its lateral–torsional buckling capacity. The maximum unbraced length relevant to lateral stability checks is obtained using Equation (21).

$$Lp = 1.76r_y\sqrt{\frac{E}{f_y}} \tag{18}$$

$$rts = \sqrt{\frac{\sqrt{I_y.c_w}}{S_z}} \tag{19}$$

$$h_0 = dc - t_f \tag{20}$$

$$Lr = 1.95rts(\frac{E}{0.7f_y})\sqrt{\frac{J.c}{s_z h_0} + \sqrt{\frac{J.C^2}{s_z h_0} + 6.76(0.7\frac{f_y}{E})^2}} \tag{21}$$

In Equations (18) to (21), the parameters are defined as follows:

- L_p: Limiting laterally unbraced length for the limit state of yielding
- L_r: Limiting laterally unbraced length for the limit state of inelastic lateral-torsional buckling

- r_y: Radius of gyration about the y-axis
- r_{ts}: Effective radius of gyration for the compression flange
- C_w: Warping constant
- S_z: Elastic section modulus about the z-axis (minor axis)
- I_y: Moment of inertia about the y-axis (minor axis)
- J: Torsional constant
- h_0: Distance between flange centroids

The plastic moment capacity of the section is evaluated to determine its flexural resistance under fully plastic stress distribution. This plastic bending capacity, which governs flexural strength checks, is computed using Equation (22). The axial compressive resistance of columns, accounting for buckling effects and material yielding, is determined using the nominal compressive strength expression shown in Equation (23). To assess column behavior under axial tension, the nominal tensile strength considering yielding and potential rupture through the net area is calculated using Equation (24).

$$\mathrm{M_p} = \mathrm{f_y Z_z} \tag{22}$$

$$\mathrm{Pcp} = 0.9\mathrm{Fcr.\,A} \tag{23}$$

$$\mathrm{Pct} = 0.9\mathrm{f_y.\,A} \tag{24}$$

In Equations (22) to (24), the parameters are defined as follows:

- M_p: plastic moment capacity of the section
- Z_z: plastic section modulus about the z-axis
- P_{cp}: nominal compressive capacity of the section
- P_{ct}: nominal tensile capacity of the section

To account for the effects of non-uniform bending moment distribution along a member, a moment gradient modifier (also known as the lateral–torsional buckling correction factor) is introduced. This coefficient refines the effective buckling capacity under varying moment diagrams and is evaluated using Equation (25).

$$Cb = \frac{12.5M_{max}}{2.5Ma_{b_{cmax}}} \tag{25}$$

In Equation (25), the parameters are defined as follows:

- C_b: the moment gradient modifier (lateral-torsional buckling modification factor)
- M_{max}: the absolute value of the maximum moment in the unbraced segment
- M_a: the absolute value of the moment at the quarter-point of the unbraced segment
- M_b: the absolute value of the moment at the centerline of the unbraced segment
- M_c: the absolute value of the moment at the three-quarter point of the unbraced segment

To evaluate the flexural strength of beam and column elements under bending, the nominal moment capacity is determined according to the section classification prescribed by steel design provisions. Depending on whether the flange and web are compact, noncompact, or slender, different expressions govern the nominal flexural capacity. The general formulation leading to these strength expressions is introduced in Equations (26_28). When both the flange and the web satisfy compactness limits, the

section is capable of developing its full plastic moment prior to the onset of local buckling. Accordingly, the nominal flexural strength is governed by the plastic moment capacity, as defined in Equation (27). For sections with a compact web but a noncompact flange, local buckling in the flange may occur before reaching the fully plastic state. In such cases, the nominal flexural strength is reduced relative to the plastic moment and must be determined using the transition equation that accounts for flange noncompactness. The corresponding expression is provided in Equation (28).

$$\begin{aligned}
&\mathrm{Lb} \le \mathrm{Lp} \rightarrow \mathrm{M_{nc}} = \mathrm{M_p} \\
&\mathrm{Lb} \le \mathrm{Lr} \rightarrow \begin{cases} \mathrm{M_{nc}} = \dfrac{\mathrm{M_p} - (\mathrm{M_p} - 0.7\mathrm{f_y})(\mathrm{Lb} - \mathrm{Lp})}{\mathrm{Lr} - \mathrm{Lp}} \\ \mathrm{M_{nc}} = \min(\mathrm{M_p}, \mathrm{M_{nc}}) \end{cases} \\
&\mathrm{Lb} > \mathrm{Lr} \rightarrow \begin{cases} \mathrm{Fcr} = \dfrac{\mathrm{Cb}.\pi^2.\mathrm{E}\sqrt{1+0.078(\frac{\mathrm{J}}{\mathrm{S_z h_0}})(\frac{\mathrm{Lb}}{\mathrm{rts}})^2}}{(\frac{\mathrm{Lb}}{\mathrm{rts}})^2} \\ \mathrm{M_{nc}} = \min(\mathrm{M_p}, \mathrm{S_z Fcr}) \end{cases}
\end{aligned} \tag{26}$$

$$\lambda_F \le \lambda_{Fp} \& \lambda_w \le \lambda_{wp} \rightarrow \mathrm{M_n} = \phi \mathrm{M_{nc}} \tag{27}$$

$$\lambda_F > \lambda_{Fp} \& \lambda_w \le \lambda_{wp} \rightarrow \mathrm{M_n} = \begin{cases} \mathrm{M_{n1}} = \mathrm{M_p} - 0.7\mathrm{f_y s_z}(\frac{\lambda_F - \lambda_{Fp}}{\lambda_{Fr} - \lambda_{Fp}}) \\ \mathrm{M_n} = \phi.\min(\mathrm{M_{n1}}, \mathrm{M_{nc}}) \end{cases} \tag{28}$$

In Equation (26), Lb represents the laterally unbraced length of the member and M_n is denotes the nominal flexural strength of the element.

For members whose flange and web do not fall into the compact or noncompact categories considered previously, the flexural strength must be evaluated using the more general expressions provided in advanced stability-based formulations. The corresponding procedure begins with the definition presented in Equation (29). A dimensionless parameter is introduced to quantify the influence of web slenderness and to support the development of subsequent reduction factors for flexural capacity. This non-dimensional factor, which forms the basis for the web slenderness reduction, is defined in Equation (30). Using the parameter introduced in the previous step, a reduction coefficient is derived to account for the decrease in nominal flexural strength caused by web slenderness. The expression for this reduction factor is given in Equation (31). For sections not fully compact, the resistance to lateral–torsional buckling depends on an effective radius of gyration that reflects the member's torsional–flexural stability characteristics. This effective radius of gyration is computed using Equation (32). The effective braced length associated with lateral-torsional stability is quantified through Equation (33). This length represents the distance between lateral bracing points that restrain the compression flange. The effective braced length associated with lateral-torsional stability is quantified through equation (33).This length represents the distance between lateral bracing points that restrain the compression flange.

Otherwise:

$$a_w = min(10, \frac{dc.t_w}{\frac{b_f}{t_f}}) \tag{29}$$

$$R_{pg} = min(1{,}1 - (\frac{a_w}{1200+300a_w})\frac{dc}{t_w} - 5.7\frac{E}{f_y}) \tag{30}$$

$$M_{n1} = \phi R_{pg} f_y S_{xc} \tag{31}$$

$$rt = \frac{b_f}{\sqrt{12(1+\frac{a_w}{6})}} \tag{32}$$

$$Lb = 1.1rt\sqrt{\frac{E}{f_y}} \tag{33}$$

$$Lr = \pi rt\sqrt{\frac{E}{\frac{0.7}{f_y}}} \tag{34}$$

In Equations (29) to (34), the parameters are defined as follows:

- a_w: a dimensionless quantity
- R_{pg}: bending strength reduction factor due to web slenderness
- S_{xc}: elastic section modulus relative to the extreme compression fiber
- r_t: effective radius of gyration for lateral-torsional buckling

When the effective braced length of the member is less than or equal to the limiting value, the section is considered sufficiently braced to prevent lateral–torsional buckling. Under this condition, the nominal flexural strength is calculated according to Equation (35). For members whose effective braced length exceeds the compact limit but remains below the maximum unbraced length, the flexural strength must be interpolated between the plastic moment and the elastic lateral–torsional buckling capacity. The corresponding expression is given in Equation (36). Since several potential limit states may control the flexural capacity (plastic rotation, web slenderness effects, lateral–torsional buckling, or flange noncompactness), the governing nominal flexural strength is taken as the minimum value among all candidate strengths. This final governing expression is documented in Equation (37).

$$if(Lb > Lp) \rightarrow \begin{cases} if(Lb < Lr) \rightarrow Fcr = min(f_y, Cb(f_y - \frac{0.3f_y(Lb-Lp)}{Lr-Lp})) \\ otherwise \rightarrow Fcr = min(f_y, \frac{Cb\pi^2E}{(\frac{Lb}{rt})^2}) \\ M_{n2} = \phi Rpg.Fcr.s_{xc} \end{cases} \tag{35}$$

$$if\lambda_F > \lambda_{Fp} \rightarrow \begin{cases} Fcr = f_y - (0.3f_y)(\frac{\lambda_F - \lambda_{Fp}}{\lambda_{Fr} - \lambda_{Fp}}) \\ M_{n3} = \phi Rpg.Fcr.s_{xc} \end{cases}$$
$$if\lambda_F < \lambda_{Fp} \rightarrow M_{n3} = Rpg.M_y \tag{36}$$

$$M_n = min(M_{n1}, M_{n2}, M_{n3}) \tag{37}$$

In Equation (36), M_y represents the yield moment of the cross-section.

To incorporate the computed flexural capacity into the optimization framework, a flexural demand-to-capacity constraint is formulated. This constraint ensures that the applied bending moment does not exceed the governing nominal strength determined previously. The mathematical form of this final flexural requirement is presented in Equation (38).

$$g_6(x_i) = M_u - M_n < 0 \tag{38}$$

In Equation (38), M_u represents the required flexural strength (factored applied moment).

The optimization process incorporates two key strength interaction constraints to address combined stress conditions. Constraint 7 ,Equation (39) defines the axial-flexural interaction for members subjected to high compressive axial loads, ensuring stability and strength under compression-dominated states. Conversely, Constraint 8 ,Equation (40) specifies the interaction criterion for members under significant tensile forces, safeguarding against tensile-yielding failures. These dual constraints collectively ensure a comprehensive strength-based design.

$$\text{if}\frac{\text{Pup}}{\text{Pcp}} \geq 0.2 \rightarrow g_7(x_i) = \left(\frac{\text{Pup}}{\text{Pcp}}\right) + \frac{8M_u}{9M_n} - 1 > 0$$

$$\text{otherwise} \rightarrow g_7(x_i) = \left(\frac{\frac{\text{Pup}}{2}}{\text{Pcp}}\right) + \frac{M_u}{M_n} - 1 > 0 \quad (39)$$

$$\text{if}\frac{\text{Put}}{\text{Pct}} \geq 0.2 \rightarrow g_8(x_i) = \left(\frac{\text{Put}}{\text{Pct}}\right) + \frac{8M_u}{9M_n} - 1 > 0$$

$$\text{otherwise} \rightarrow g_8(x_i) = \left(\frac{\frac{\text{Put}}{2}}{\text{Pct}}\right) + \frac{M_u}{M_n} - 1 > 0 \quad (40)$$

In Equations (39) and (40), the following parameters are defined:

- P_{ut}: the factored applied tensile axial force
- P_{up}: the factored applied compressive axial force

To satisfy serviceability and damage-control requirements, Constraint 9 Equation (41) limits the maximum computed inter-story drift ratio to the code-specified allowable value, thereby controlling structural deformations under seismic actions.

$$g_9(x_i) = \delta all_{max} \quad (41)$$

In Equation (41), the parameters are defined as follows:

- δ_{all}: the allowable story drift, taken as 0.02 times the story height,
- δ_{max}: the maximum computed story drift under design loads,
- C_d: the deflection amplification factor accounting for inelastic deformations.

3. Results and Discussion

This section presents the numerical results of the optimization procedure and discusses their implications for the seismic performance of steel frames equipped with Strongback bracing systems. The results are organized as follows: first, the adopted computational framework is verified against available studies to ensure reliability; second, the optimization outcomes for the three Strongback configurations are reported and compared, both with and without the drift uniformity constraint; finally, the significance of the proposed constraint and its influence on structural efficiency and seismic response are analyzed.

3.1. Optimization Results

The optimization procedure was applied to the six story steel frame equipped with three different Strongback configurations, namely brace to beam intersections at one quarter ($\frac{1}{4}$), one third ($\frac{1}{3}$), and five twelfths ($\frac{5}{12}$) of the beam span. For each configuration, two cases were analyzed: (i) without the inter story drift uniformity constraint, and (ii) with the drift uniformity constraint included in the optimization process.

The optimized cross sectional sizes assigned to each member group are presented in Table 3 for the three brace intersection configurations ($\frac{1}{4}$, $\frac{1}{3}$, and $\frac{5}{12}$ span), both with and without the drift uniformity constraint.

As shown in Table 3, the optimization outcomes reflect geometry dependent stiffness redistribution, indicating how the drift uniformity constraint directly influences sectional design decisions across different Strongback configurations.

Table 3. Optimized cross sectional areas (m²) of 19 member groups under different Strongback configurations ($\frac{1}{4}$, $\frac{1}{3}$, and $\frac{5}{12}$ span), with and without the DUF.

Number of group	$\frac{1}{3}$ span		$\frac{1}{4}$ span		$\frac{5}{12}$ span	
	Area sections without DUF constraint	Area sections with DUF constraint	Area sections without DUF constraint	Area sections with DUF constraint	Area sections without DUF constraint	Area sections with DUF constraint
1	0.0650	0.0735	0.0703	0.0589	0.0399	0.0677
2	0.0195	0.0257	0.0304	0.0257	0.0347	0.0467
3	0.0671	0.0499	0.0650	0.0634	0.0552	0.0684
4	0.0671	0.0671	0.0448	0.0498	0.0925	0.0579
5	0.0735	0.0362	0.0303	0.0279	0.04	0.0468
6	0.0328	0.0281	0.0281	0.0498	0.0498	0.0467
7	0.0459	0.0365	0.0421	0.0498	0.0468	0.0439
8	0.0381	0.0367	0.0307	0.0619	0.0619	0.0400
9	0.0106	0.0058	0.0101	0.007	0.007	0.0086
10	0.0065	0.0065	0.0155	0.0160	0.0201	0.0184
11	0.0367	0.0159	0.0117	0.0141	0.0121	0.0075
12	0.0118	0.0094	0.0128	0.0105	0.0101	0.0128
13	0.0144	0.0101	0.0072	0.0103	0.0087	0.0129
14	0.0247	0.0221	0.0105	0.0057	0.0094	0.0135
15	0.0121	0.0087	0.0121	0.0146	0.0139	0.0101
16	0.0121	0.0106	0.0057	0.0040	0.0074	0.0051
17	0.0087	0.0076	0.0101	0.0053	0.0066	0.0074
18	0.0034	0.0017	0.0011	0.0013	0.0023	0.0017
19	0.0026	0.0057	0.0014	0.0023	0.003	0.0026

The results in Table 3 reveal clear trends in the redistribution of material among member groups due to the application of the DUF. In general, the inclusion of the DUF constraint led to an increase in the cross sectional areas of critical members responsible for lateral stiffness particularly in the upper and mid story bracing and beam groups while slightly reducing the sizes of non critical members. This behavior indicates that the optimization algorithm compensated for the drift uniformity requirement by strengthening regions contributing to inter story stiffness balance, rather than uniformly increasing all member sizes.

For the one third and one fourth span configurations, the adjusted section areas demonstrate a more efficient stiffness allocation, leading to reduced total structural weight despite the added constraint. This confirms that the DUF constraint enhanced the coordination of stiffness demand along the height of the structure. Conversely, in the five twelfths configuration, most member areas increased simultaneously,

reflecting a less favorable stiffness path between the Strongback and frame elements. This geometric inefficiency caused a net rise in the optimized structural weight.

Overall, Table 3 highlights that the proposed drift uniformity constraint not only improves deformation regularity but also promotes rational material distribution, enhancing both mechanical performance and design efficiency.

In contrast, incorporating the drift uniformity constraint resulted in larger and more uniformly distributed member sections along the building height. This adjustment indicates that the algorithm effectively increased the stiffness of the upper and mid story members to achieve a more consistent lateral deformation profile. Among the three brace to beam intersection configurations, the one fourth span layout demonstrated the most balanced pattern of section sizes, achieving improved drift uniformity with only a moderate increase in member dimensions.

To further illustrate the influence of the DUF on lateral deformation patterns, Figure 6 presents the inter-story drift profiles for the three brace-to-beam intersection configurations ($\frac{1}{4}$, $\frac{1}{3}$, and $\frac{5}{12}$) under scenarios with and without the DUF constraint.

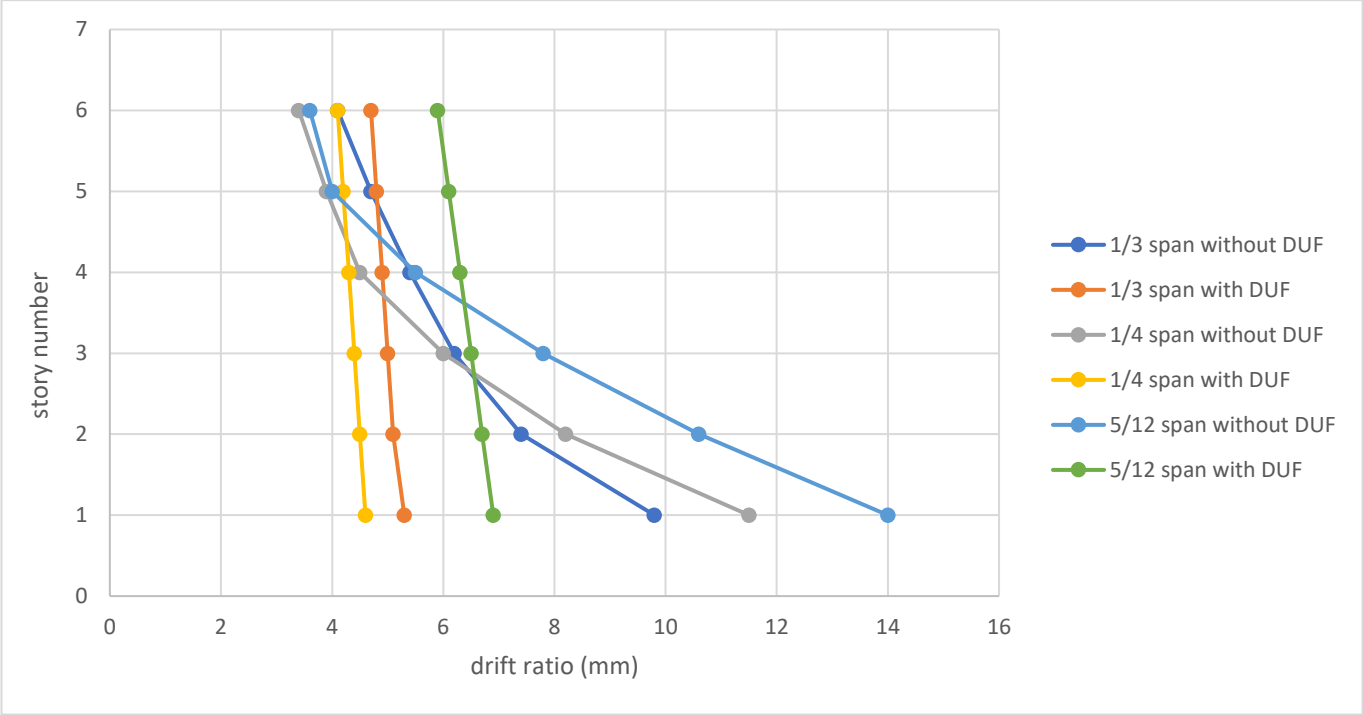

Fig. 6. Inter-story drift profiles for the three Strongback configurations ($\frac{1}{4}$, $\frac{1}{3}$, and $\frac{5}{12}$span ratios) with and without the DUF constraint.

As shown in Figure 6, the drift demand in the "without-DUF" cases exhibits the typical concentration in the lower stories, a behavior commonly associated with soft-story tendencies in braced frames. Introducing the DUF constraint significantly regularizes the drift profile across the height, producing nearly uniform drift values for all three configurations. The $\frac{1}{4}$-span configuration achieves the most balanced distribution with the lowest drift concentration, whereas the $\frac{5}{12}$-span configuration remains the least uniform, even under DUF enforcement consistent with its higher optimized weight and reduced stiffness redistribution efficiency. These drift trends provide clear physical insight into the role of brace-to-beam geometry in controlling lateral deformation patterns within Strongback systems.

A comparison of the optimized total weights under the three brace to beam intersection ratios is given in Table 4.

As observed, the inclusion of the drift uniformity constraint results in a weight reduction of approximately 2.48%, 6.96% for the one third and one fourth span configurations, while a slight increase (14.92%) is observed for the five twelfths span layout. The summary of the total optimized weights for the three Strongback configurations, with and without the drift uniformity constraint, is presented in Table 4.

Table 4. Comparison of optimized total structural weights for different Strongback configurations, with and without the DUF.

Brace to Beam Intersection Ratio	Optimum weight with considering drift uniformity index (kg)	Optimum weight without considering drift uniformity index (kg)
$\frac{1}{3}$ span	90802.224	93111.9374
$\frac{1}{4}$ span	87165.4955	93686.7541
$\frac{5}{12}$ span	121976.5752	106137.0903

Table 4 shows the optimized weights for different brace to beam intersection configurations, both with and without the drift uniformity constrain. As summarized in Table 4, the drift uniformity constraint yielded geometry dependent effects on optimized weight, highlighting the nonlinear interaction between stiffness distribution and global efficiency.The results indicate that the GA was successful in identifying optimal section sizes that satisfy all design constraints while minimizing the structural weight. In the absence of the drift uniformity constraint, the optimization converged to lighter solutions; however, the drift distribution along the height of the frame was highly non uniform, with concentration of deformations in upper stories. When the drift uniformity constraint was enforced, the structural weight generally increased, but the drift profile became significantly more uniform, leading to improved seismic performance and better energy dissipation capacity.

Among the three Strongback configurations, the brace to beam intersection at one fourth ($\frac{1}{4}$) of the span exhibited the most favorable trade off between weight reduction and drift uniformity, while the configuration at five twelfths ($\frac{5}{12}$) of the span showed limited weight reduction when the drift uniformity constraint was imposed. This suggests that the geometric location of the Strongback plays a critical role in balancing stiffness, strength, and drift control.

To assess the convergence stability and computational efficiency of the optimization process, the evolution of the objective function value (structural weight) with the number of generations is presented in Figure 7. Both constrained and unconstrained optimization cases are shown for all three brace intersection configurations.

It was observed that the $\frac{5}{12}$ brace-to-beam intersection led to a noticeably higher optimized weight when the DUF constraint was applied. This behavior can be attributed to the mechanical characteristics of this configuration. The $\frac{5}{12}$ position lies closer to the beam mid-span, where flexural demand is highest and shear transfer effectiveness is reduced. As a result, the coupling between axial brace forces and lateral story shear becomes weaker, limiting the ability of the Strongback system to redistribute stiffness efficiently along the frame height. To satisfy the DUF constraint under this less effective force-transfer mechanism, the optimization process increases the brace and column sizes more substantially than in the $\frac{1}{4}$ and $\frac{1}{3}$ configurations. Therefore, the higher weight of the $\frac{5}{12}$ geometry arises not only from its geometric characteristics but from this inherent mechanical limitation.

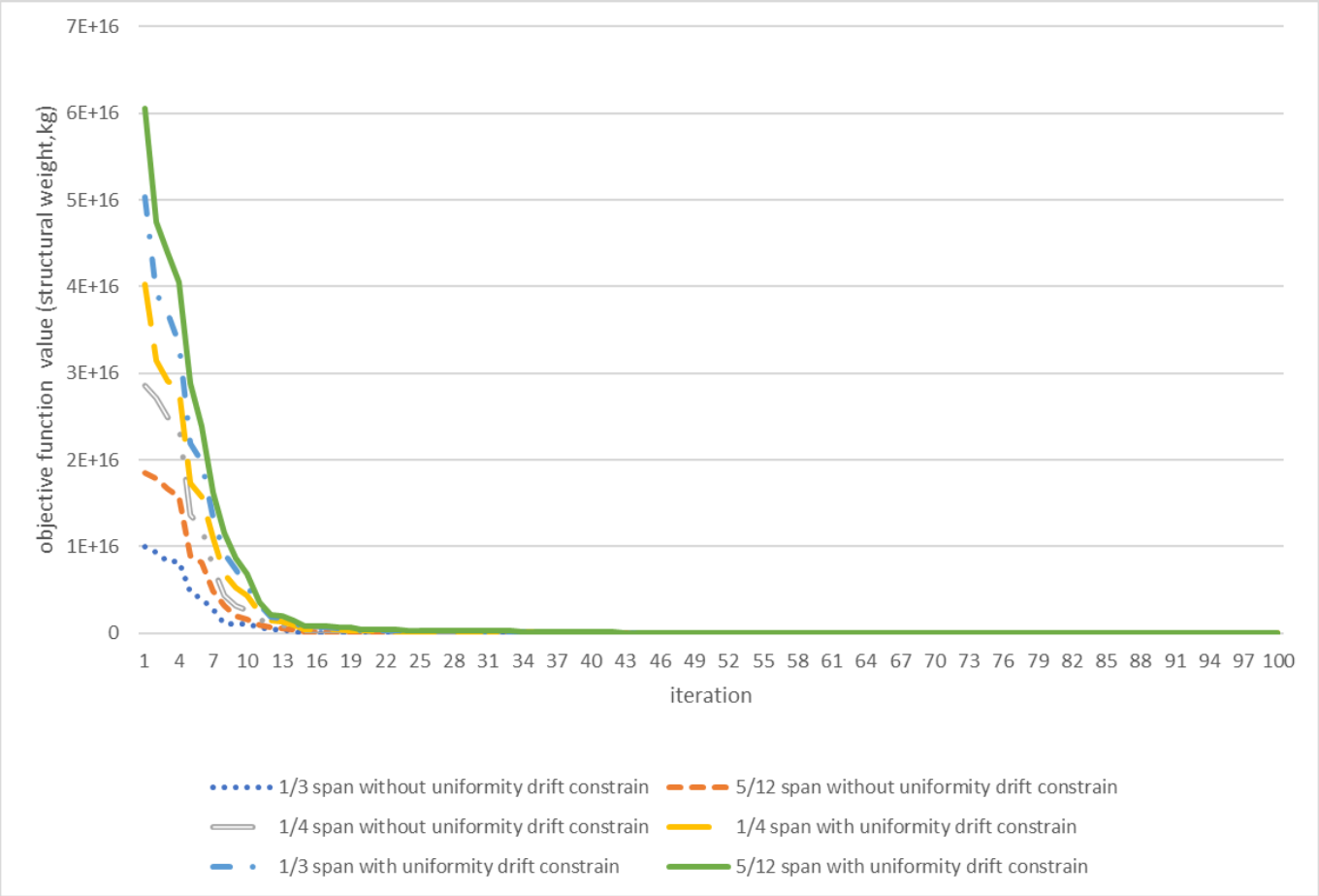

Fig. 7. Convergence histories of the GA for the six-story Strongback frame under the three brace-to-beam intersection ratios ($\frac{1}{4}$, $\frac{1}{3}$, $\frac{5}{12}$), with and without the DUF constraint.

As illustrated in Figure 7, all optimization scenarios exhibit stable and rapid convergence behavior, confirming the robustness of the Genetic Algorithm implementation. For both constrained and unconstrained cases, the objective function (structural weight) decreases sharply during the first 30–50 iterations, after which the changes become negligible, indicating that near optimal solutions were reached well before the maximum iteration count of 100.

In the unconstrained optimizations, the minimum structural weights stabilized at approximately 9.3×10^4 kg for both the $\frac{1}{3}$ span and $\frac{1}{4}$ span configurations, and 1.06×10^5 kg for the $\frac{5}{12}$ span configuration. This confirms that, without the drift uniformity constraint, the optimization primarily focuses on minimizing weight without regard to lateral stiffness distribution.

When the drift uniformity constraint was introduced, the convergence rate remained nearly identical, showing that the additional constraint did not compromise computational efficiency. However, its influence on final weight varied depending on brace geometry. For the $\frac{1}{3}$ span and $\frac{1}{4}$ span layouts, the optimized weights slightly decreased to about 8.8×10^4 kg and 9.0×10^4 kg, respectively, indicating more efficient stiffness distribution due to the imposed drift constraint. In contrast, for the $\frac{5}{12}$ span configuration, the final weight increased to approximately 1.25×10^5 kg, implying that this geometry generates redundant stiffness that does not effectively contribute to drift uniformity.

Overall, the convergence histories demonstrate that all optimization cases achieved steady state solutions within roughly 50 generations, verifying the stability, consistency, and computational efficiency of the developed GA–OpenSees optimization framework. Moreover, the distinct trends among the three brace

configurations quantitatively confirm the strong dependency of optimal performance on brace placement geometry. The results summarized in Tables 3 and 4 form the basis for the following discussion, which interprets the observed trends in light of stiffness distribution and drift control.

3.2. Discussion

The optimization results highlight the crucial role of the drift uniformity constraint in achieving efficient and resilient Strongback braced steel frames. Conventional optimization approaches that minimize only the total weight typically yield lighter but mechanically unbalanced designs, characterized by pronounced concentration of inter story drifts in the upper levels. Such irregular drift distributions may trigger soft story mechanisms and lead to premature local failures during seismic excitation. The incorporation of the proposed drift uniformity constraint effectively mitigates these shortcomings by enforcing a more balanced redistribution of stiffness along the structure's height, thereby reducing the concentration of deformations in specific stories and preventing localized drift failures.

A particularly noteworthy outcome of this study is the unexpected reduction in optimized structural weight observed for the one third and one fourth span configurations when the drift uniformity constraint was applied. At first glance, adding a new constraint is generally expected to restrict the solution space and increase the objective value (i.e., total weight). However, in this case, the drift uniformity requirement indirectly improved the overall efficiency of stiffness allocation For the $\frac{1}{3}$ span configuration, the structural weight unexpectedly decreased by 3.5% after applying the uniformity constraint. This occurred because, the optimization algorithm naturally favored section combinations that provided better stiffness coordination between stories, thereby eliminating over stiffness in localized regions that existed in unconstrained solutions. This redistribution of stiffness reduced redundant material usage, leading to lighter yet more mechanically efficient designs. This behavior reveals that the drift constraint can act as an implicit stiffness regularizer, guiding the optimization toward structurally more balanced solutions.

In contrast, the five twelfths span configuration exhibited an increase in total weight when the same constraint was applied. This specific configuration saw a weight increase of 14.96%, a behavior which can be attributed to its less effective geometric interaction between the Strongback brace and the surrounding frame members, which limits the system's capacity to redistribute stiffness without adding material. Consequently, the optimization algorithm compensated for the drift uniformity requirement through the selection of heavier sections, resulting in an increased total weight. This finding is consistent with the observations by Faramarzi and Taghikhany [30], who also reported geometry dependent drift uniformity in Strongback frames.

Overall, the results demonstrate that the effectiveness of the drift uniformity constraint is geometry dependent: when the brace to beam intersection occurs at positions that promote favorable stiffness coupling such as at one third or one fourth of the beam span the constraint enhances both performance and material efficiency. However, in suboptimal geometries (e.g., the five twelfths configuration), the constraint imposes additional stiffness demands that increase material consumption.

These findings also reaffirm the capability of the GA to manage multi objective optimization landscapes involving nonlinear interdependencies between stiffness, strength, and deformation. The observed convergence behavior indicates that the GA consistently identifies near optimal solutions within fewer than 100 generations, validating its robustness and computational efficiency for discrete structural optimization. Future research could further refine these insights by incorporating nonlinear static and dynamic analyses to investigate post yield behavior, residual drift, and energy dissipation mechanisms under realistic seismic scenarios.These findings suggest that the proposed framework can be integrated into preliminary design tools for drift controlled and weight efficient optimization of steel braced frames.

Uncertainties associated with material properties, geometric variability, and model idealization were not explicitly modeled. Future work will incorporate sensitivity and uncertainty propagation to examine robustness of the optimization results.

A clearer relationship between geometry and seismic indicators emerges: configurations with lower brace-to-beam ratios suppress soft-story formation more effectively, reduce drift concentration, and achieve a more favorable deformation pattern. This behavior aligns with the mechanics of stiffness redistribution and the role of the vertical spine in Strongback systems

4. Conclusions

This study presented a discrete size optimization framework for six story steel frames equipped with Strongback bracing systems, with particular emphasis on inter story drift uniformity as a novel design constraint. The optimization was performed using a Genetic Algorithm integrated with OpenSees for structural analysis. Based on the results, the following conclusions can be drawn:

1. **Effectiveness of Drift Uniformity Constraint** – Incorporating drift uniformity significantly improves the seismic performance of Strongback systems by preventing excessive concentration of deformations in individual stories, thereby reducing the risk of soft story collapse mechanisms.
2. **Impact of Strongback Configuration** – Among the three investigated configurations, the one fourth span intersection consistently provided the best balance between weight efficiency and drift uniformity. In contrast, the five twelfths configuration showed limited weight reduction under the uniformity constraint, indicating that geometric placement plays a critical role in Strongback effectiveness.
3. **Optimization Efficiency** – The proposed GA based framework proved effective in handling the discrete design space and multiple performance constraints, achieving near optimal solutions within a reasonable number of generations.
4. **Practical Implications** – The findings demonstrate that Strongback systems, when properly optimized, can provide improved seismic resilience with only a modest increase in structural weight, making them an attractive option for performance based design of steel frames.
5. **Future Work** – While the present study focused on linear static analysis, future research should incorporate nonlinear time history simulations and additional performance criteria, such as residual drift and energy dissipation, to further validate the robustness of the proposed methodology.

Overall, the proposed framework provides a practical and computationally efficient tool for drift controlled design of steel Strongback frames, offering a promising basis for future extensions toward nonlinear and performance oriented analyses.

While the numerical findings are directly associated with the six-story benchmark frame, the observed behavioral trends are expected to extend to taller configurations. Nevertheless, the current results should be interpreted within the specific modeling assumptions adopted.

The key findings of this study can be summarized as follows:

- A GA integrated with OpenSees was successfully implemented to optimize Strongback braced frames under linear static analysis while enforcing multiple design constraints, including a newly introduced drift-uniformity constraint.
- The optimization results revealed that geometric configuration plays a decisive role in the seismic behavior of Strongback systems. The brace-to-beam intersection ratios ($\frac{1}{4}$, $\frac{1}{3}$, $\frac{5}{12}$of the span) produced distinct drift and weight distribution patterns.

- In the unconstrained optimization, differences in total structural weight between configurations were modest (0.61% between $\frac{1}{3}$and $\frac{1}{4}$ spans; 12.27% between $\frac{1}{3}$ and $\frac{5}{12}$; 11.73% between $\frac{1}{4}$ and $\frac{5}{12}$).
- When the drift-uniformity constraint was applied, these differences increased to 4.17%, 25.56%, and 28.55%, respectively highlighting the strong sensitivity of Strongback action to geometric layout.
- The drift-uniformity constraint led to weight reductions of 2.47% ($\frac{1}{4}$ span) and 6.95% ($\frac{1}{3}$ span), while the $\frac{5}{12}$ span configuration experienced a moderate weight increase of 14.96%.
- Across all configurations, the drift-uniformity constraint substantially improved drift distribution, demonstrating its effectiveness as a novel and practical design feature for enhancing seismic performance.
- The comparative analysis indicates that the $\frac{1}{3}$-span configuration consistently offers the most favorable balance between drift uniformity and total structural weight.
- The findings establish that incorporating a drift-uniformity constraint into optimization frameworks can provide a systematic and performance-oriented strategy for selecting Strongback configurations in seismic design.

The study is subject to limitations related to linear analysis assumptions, idealized material modeling, and exclusion of record to record ground motion variability

This work demonstrates that introducing a drift-distribution constraint provides a new pathway for performance-based optimization.

Future research will involve nonlinear time-history simulations to evaluate residual inter-story drift, inelastic drift distribution, and plastic hinge development, providing a more comprehensive validation of the proposed drift-uniformity constraint.

Finally, it should be noted that the present results are obtained under linear static assumptions and therefore represent a preliminary, design-level assessment. Future developments of the framework will involve incorporating nonlinear static and time-history analyses to validate the DUF in fully inelastic regimes and to adapt the constraint formulation for controlling residual drifts and energy dissipation under severe earthquakes.

Funding

This research did not receive any specific grant from funding agencies in the public, commercial, or not-for-profit sectors.

Conflicts of interest

The authors declare that they have no known competing financial interests or personal relationships that could have appeared to influence the work reported in this paper.

Authors contribution statement

Ehsan Jahankhani: Methodology, Investigation, Software, Resources, Data curation, Formal analysis, Writing – original draft, Funding acquisition.

Omid Rezaifar: Conceptualization, Validation, Supervision, Writing – review & editing.

Majid Gholhaki: Conceptualization, Supervision, Writing – review & editing.

Peyman Homami: Supervision, Writing – review & editing.

References

[1] AISC 341-10 - American Institute of Steel Construction. Seismic Provisions for Structural Steel Buildings. 2010.

[2] Fema P. 58-1, Seismic performance assessment of buildings volume 1-methodology. Appl Technol Counc Calif Redw City 2012.

[3] Simpson BG, Mahin SA. Experimental and numerical investigation of strongback braced frame system to mitigate weak story behavior. J Struct Eng 2018;144:4017211. https://doi.org/10.1061/(ASCE)ST.1943-541X.0001960.

[4] Toorani A, Gholhaki M, Vahdani R. The investigation into the effect of consecutive earthquakes on the strongback bracing system. Structures, vol. 24, Elsevier; 2020, p. 477–88. https://doi.org/10.1016/j.istruc.2020.01.018.

[5] Lai J-W, Mahin SA. Strongback system: A way to reduce damage concentration in steel-braced frames. J Struct Eng 2015;141:4014223.

[6] Simpson B, Mahin S. Design development of a four-story Strongback braced frame. Key Eng Mater 2018;763:1050–7. https://doi.org/10.4028/www.scientific.net/KEM.763.1050.

[7] Bagley JD. The behavior of adaptive systems which employ genetic and correlation algorithms: technical report 1967.

[8] Goldberg DE. Genetic algorithms as a computational theory of conceptual design. Appl. Artif. Intell. Eng. VI, Springer; 1991, p. 3–16.

[9] Wu S-J, Chow P-T. Integrated discrete and configuration optimization of trusses using genetic algorithms. Comput Struct 1995;55:695–702.

[10] Rafiq MY, Southcombe C. Genetic algorithms in optimal design and detailing of reinforced concrete biaxial columns supported by a declarative approach for capacity checking. Comput Struct 1998;69:443–57.

[11] Kameshki ES, Saka MP. Optimum design of nonlinear steel frames with semi-rigid connections using a genetic algorithm. Comput Struct 2001;79:1593–604.

[12] Balling RJ, Briggs RR, Gillman K. Multiple optimum size/shape/topology designs for skeletal structures using a genetic algorithm. J Struct Eng 2006;132:1158–65. https://doi.org/10.1061/(ASCE)0733-9445(2006)132:7(1158).

[13] Cui H, An H, Huang H. Truss topology optimization considering local buckling constraints and restrictions on intersection and overlap of bar members. Struct Multidiscip Optim 2018;58:575–94. https://doi.org/10.1007/s00158-018-1910-x.

[14] Rao GV. Optimum designs for transmission line towers. Comput Struct 1995;57:81–92. https://doi.org/10.1016/0045-7949(94)00597-V.

[15] Hasançebi O. Adaptive evolution strategies in structural optimization: Enhancing their computational performance with applications to large-scale structures. Comput Struct 2008;86:119–32. https://doi.org/10.1016/j.compstruc.2007.05.012.

[16] Geem ZW, Kim JH, Loganathan GV. A new heuristic optimization algorithm: harmony search. Simulation 2001;76:60–8.

[17] Kaveh A, Talatahari S. Particle swarm optimizer, ant colony strategy and harmony search scheme hybridized for optimization of truss structures. Comput Struct 2009;87:267–83. https://doi.org/10.1016/j.compstruc.2009.01.003.

[18] Jahankhani E, Asadollahfardi G, Samadi A. Toward sustainable water quality monitoring systems using particle swarm, Ant Colony, and Tabu Search optimization methods. Qual Quant 2024;58:2957–77. https://doi.org/10.1007/s11135-023-01781-x.

[19] Panian L, Bucci N, Janhunen B. BRBM frames: An improved approach to seismic-resistant design using buckling-restrained braces. Improv. Seism. Perform. Exist. Build. Other Struct. 2015, 2015, p. 632–43. https://doi.org/10.1061/9780784479728.052.

[20] Laghi V, Palermo M, Gasparini G, Trombetti T. Strong-back system coupled with framed structure to control the building seismic response. J Civ Environ Eng 2017;7:1–7. https://doi.org/10.4172/2165-784x.1000274.

[21] Laghi V, Palermo M, Gasparini G, Silvestri S, Trombetti T. Strongback system to enhance the building seismic response of framed structures. Atti Del XVII Convegno ANIDIS L'ingegneria Sismica Ital Pist 17-21 Settembre 2017-(Studi Tema Di Internet Ecosyst 2017:72–81.

[22] Liu J. Steel Structures Research Update: Strongback Steel-Braced Frames for Improved Seismic Behavior in Buildings. Eng J 2017;54:297–308. https://doi.org/10.62913/engj.v54i4.1120.

[23] Palermo M, Laghi V, Gasparini G, Trombetti T. Coupled response of frame structures connected to a strongback. J Struct Eng 2018;144:4018148. https://doi.org/10.1061/(asce)st.1943-541x.0002134.

[24] Talley PC. Capacity design methods for strongback braced frames 2018.

[25] Lin J-L, Kek M-K, Tsai K-C. Stiffness configuration of strongbacks to mitigate inter-story drift concentration in buildings. Eng Struct 2019;199:109615. https://doi.org/10.1016/j.engstruct.2019.109615.

[26] Faramarzi MS, Taghikhany T. Direct performance-based seismic design of strongback steel braced systems. Structures, vol. 28, Elsevier; 2020, p. 482–95. https://doi.org/10.22060/ceej.2025.23688.8197.

[27] Simpson BG. Higher-mode force response in multi-story strongback-braced frames. Earthq Eng Struct Dyn 2020;49:1406–27. https://doi.org/10.1002/eqe.3310.

[28] Jahangir H, Bagheri M. Evaluation of seismic response of concrete structures reinforced by shape memory alloys. Int J Eng 2020;33:410–8. https://doi.org/10.5829/IJE.2020.33.03C.05.

[29] Jahangir H, Bagheri M, Delavari SMJ. Cyclic behavior assessment of steel bar hysteretic dampers using multiple nonlinear regression approach. Iran J Sci Technol Trans Civ Eng 2021;45:1227–51. https://doi.org/10.1007/s40996-020-00497-4.

[30] Faramarzi MS, Taghikhany T. A comparative performance-based seismic assessment of strongback steel braced frames. J Build Eng 2021;44:102983. https://doi.org/10.1016/j.jobe.2021.102983.

[31] Astudillo B, Panian L, Simpson B. Design and Performance Comparison of Strongback Systems and Typical Chevron BRB Frames. 12th Natl Conf Earthq Eng 2022.

[32] Abolghasemi S, Wierschem NE, Denavit MD. Impact of strongback on structure with varying damper and stiffness irregularity arrangements. J Constr Steel Res 2024;213:108333. https://doi.org/10.1016/j.jcsr.2023.108333.

[33] Soleymani A, Saffari H. A novel hybrid strong-back system to improve the seismic performance of steel braced frames. J Build Eng 2024;84:108482. https://doi.org/10.1016/j.jobe.2024.108482.

[34] Gholhaki M, Gorji Azandariani M, Hooshdar Rostami A, Rezaifar O. Seismic Retrofit and Strengthening of Reinforced Concrete Moment Frames with Strongback-Braced System. Pract Period Struct Des Constr 2024;29:4024005. https://doi.org/10.1061/PPSCFX.SCENG-1407.

[35] Ghasemi Jouneghani H, Nouri Y, Mortazavi M, Haghollahi A, Memarzadeh P. Seismic performance factors of elliptic-braced frames with rotational friction dampers through IDA. Pract Period Struct Des Constr 2024;29:4024070. https://doi.org/10.1061/PPSCFX.SCENG-1540.

[36] Ghasemi Jouneghani H, Nouri Y, Memarzadeh P, Haghollahi A, Hemati E. Seismic performance and failure mechanisms evaluation of multi-story elliptic and mega-elliptic bracing frames: Experimental and numerical investigation. Structures 2024;70:107658. https://doi.org/https://doi.org/10.1016/j.istruc.2024.107658.

[37] Saffarzadeh K, Saffari H, Soleymani A. Development of loading protocols for different structural systems. Innov Infrastruct Solut 2025;10:1–19. https://doi.org/10.1007/s41062-025-02340-z.

[38] Nouri Y, Jouneghani HG, Haghollahi A, Memarzadeh P, Hemati E. Experimental and numerical study of seismic performance and failure mechanisms of multi-story elliptic and Quasi-X braced resisting frames. Results Eng 2025;26:105657. https://doi.org/https://doi.org/10.1016/j.rineng.2025.105657.

[39] Nouri Y, Ghasemi Jouneghani H, Shirkhani A, Hemati E, Hemati SA, Hajirasouliha I. Seismic retrofit of steel moment frames with arc and ring yielding dampers: A probabilistic loss assessment using FEMA P-58. Structures 2025;76:108898. https://doi.org/https://doi.org/10.1016/j.istruc.2025.108898.

[40] FEMA P. 695; Federal Emergency Management Agency (FEMA). Quantif Build Seism Perform Factors Appl Technol Counc Washington, DC, USA 2009.

[41] Jouneghani HG, Nouri Y, Roudbaraki R, Haghollahi A, Hemati E. Evaluating seismic performance factors of mega elliptic-braced moment resisting frames (MEL BRFs) with FEMA P695 methodology. J Build Eng 2025;111:113511. https://doi.org/https://doi.org/10.1016/j.jobe.2025.113511.

[42] PayamiFar T, Sojoudizadeh R, Azizian H, Rahimi L. Seismic Optimization of Steel Mega-Braced Frame With Improved Prairie Dog Metaheuristic Optimization Algorithm. Struct Des Tall Spec Build 2025;34:e2207. https://doi.org/10.1002/tal.2207.

[43] No S. 2800 (2015) of Iranian Code of Practice for Seismic Resistance Design of Buildings 2015.

[44] Prestandard F. commentary for the seismic rehabilitation of buildings (FEMA356). Washington, DC Fed Emerg Manag Agency 2000;7:518.